Rotor Impedance of the High Frequency Circulating Bearing Current Path in Inverter-Fed AC Machines

Oliver Magdun, Yves Gemeinder and Andreas Binder, Senior Member IEEE,
Institute for Electrical Energy Conversion
Darmstad University of Technology
Darmstadt, Germany

***Abstract*—The circulating bearing current depends on the common mode stator ground current and the stator laminated core impedance, but also on the bearing impedances and on the rotor impedance of the circulating bearing current path. In the literature, the rotor impedance was neglected, or it was considered as a small air gap and end-winding cavity inductance. It is shown here by calculation and measurement that the rotor impedance is not negligible, and it is much larger than the air gap and end-winding cavity inductance. Moreover, it is shown that the circulating bearing currents can be mitigated, if the rotor impedance is increased by at least ten times the stator impedance. For increasing the rotor impedance, nanocrystalline magnetic materials are added on the machine shaft. The circulating bearing currents are measured for a standard 110 kW machine and for the same machine with the increased rotor impedance.**

I. INTRODUCTION

The high-frequency circulating bearing currents, apart from the rotor ground currents via the bearings, are considered to be the most destructive currents for the bearings of the large inverter-fed AC machines [1]-[4]. The source of the circulating bearing current is the common mode current i_{com}, which flows through the stator lamination yoke and excites the common mode flux ϕ_{com} in the stator yoke (Fig. 1a). The flux ϕ_{com} induces the voltage v_{SH} along the shaft that may surpass the insulating properties of the bearing lubricants and causes the circulating bearing current i_b in the loop "stator yoke – drive-end (DE) bearing & end shield – rotor shaft – non-drive-end (NDE) bearing & end shield - stator yoke" (Fig. 1b). Due to the skin effect, the circulating bearing current flows in the stator yoke at the surface of each sheet of lamination. In the rotor it flows at the outer surface, where a conductive path at the adjacent lamination sheets exists because of the resurfacing process of the cage rotor for adjusting the small air gap [4]. The stator and rotor laminated cores introduce their impedances on the circulating bearing current path, which depend on the machine size and the manufacturing process. The circulating bearing current varies not only with the stator and rotor impedances, but also with the bearing load, bearing temperature and speed, and therefore, with the bearing impedance. When the circulating bearing current flows inside the machine, the bearings may be electrically represented as small resistances, in general less than a few ohms, which depend on the bearing lubricant properties at the contact surfaces between the roller elements and the bearing race [2].

The rotor impedance was neglected in the literature or it was considered as a small air gap and end-winding cavity inductance [4] – [6]. In this paper, it is shown that for the standard cage induction machines, the rotor impedance is not negligible and may be equal to the stator impedance. Moreover, it is shown that the circulating bearing currents can be mitigated, if the rotor impedance is increased. For that, a magnetic nanocrystalline ring with high impedance at high frequency is mounted around the machine shaft at the NDE side. The effectiveness of the magnetic shaft ring is proved by measuring the circulating bearing current for a standard four-pole 110 kW induction cage machine and for the same machine with the increased rotor impedance. According to our knowledge, results of this kind of bearing current mitigation method have not been presented yet in the literature.

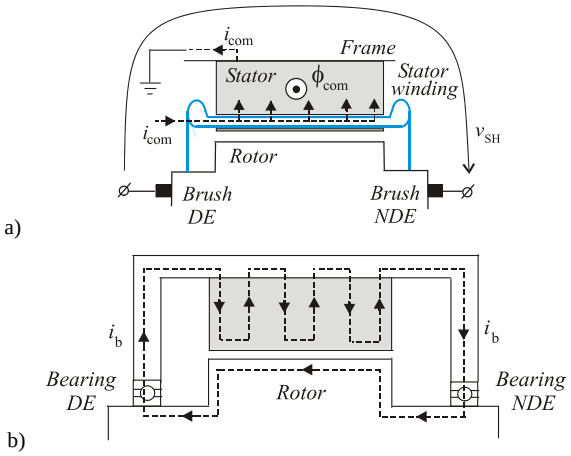

Figure 1. a) – The common mode current i_{com}, the common mode flux ϕ_{com} and the shaft voltage v_{SH}, b) – The path of the circulating bearing current i_b in inverter-fed AC machines.

This work was supported in part by Deutsche Forschungsgemeinschaft DFG, FOR575 "High-frequency parasitic effects in inverter-fed electrical drives". The financial support of Magnetec GmbH is gratefully acknowledged by the authors.

II. Measurements of Circulating Bearing Currents and Common Mode Currents

The common mode currents and the circulating bearing currents are measured for three inverter-fed four-pole cage induction machines of 110 kW and 240 kW with the data of Table I. The measurement setup is presented in Fig. 2. The common mode stator ground current was measured with a current probe, which was directly connected on the protective earth conductor. Additional paths of the common mode currents to the ground were prevented by insulating the machine frame from the ground. For measuring the circulating bearing current, an insulating layer and a bypass conductor loop were prepared at the machine end-shields (Fig. 3). For assessing the outer bearing temperature, a temperature sensor was mounted at the inner end-shield surface. The circulating bearing current was measured on the bypass conductor with a current probe with the maximum admissible frequency of 50 MHz. The 110 kW machines M1 (single layer winding) and M2 (double layer winding) are equipped with standard bearings type 6316 C3.

TABLE I. Data of the Tested 4-pole Cage Induction Machines

Machines	P_N kW	N_{lam} -	d_{se} m	d_{si} m	h_s mm	σ_{Fe} MS/m
M1	110	620	0.460	0.295	35.0	2.8
M2	110	690	0.465	0.295	39.75	3.3
M3	240	522	0.490	0.310	28.6	2.6

(N_{lam} is the number of lamination sheets, d_{se} is the stator outer diameter, d_{si} is the stator inner diameter, h_s is the stator slot height and σ_{Fe} is the iron conductivity)

Figure 2. Measurement setup for the common mode and circulating bearing currents.

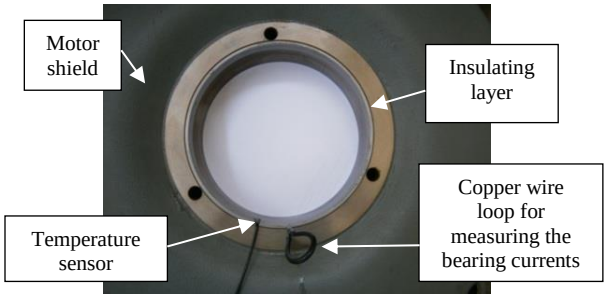

Figure 3. Preparing the motor end-shields for measuring the circulating bearing currents.

The 240 kW machine M3 (double layer winding) is equipped with insulated oxide layer bearings, type NU228-C3 at DE and 6316-C4 at NDE. For this machine bypass conductors were mounted between the stator frame and the outer bearing races to bridge the oxide layer insulation. Fig. 4, 5 and 6 show the measured common mode and circulating bearing current for the three machines of Table I. Generally, the circulating bearing current i_b follows the common mode current i_{com} waveform. In the worst case (Fig. 4), the ratio between the circulating bearing current amplitude $\hat{i}_b$ and the common mode current amplitude $\hat{i}_{com}$ is $\left|\hat{i}_b/\hat{i}_{com}\right| \cong 0.9$. This is almost twice larger than the typical values of the bearing current ratio of the induction cage machines: $\left|\hat{i}_b/\hat{i}_{com}\right| < 0.5$, as they were measured in [4].

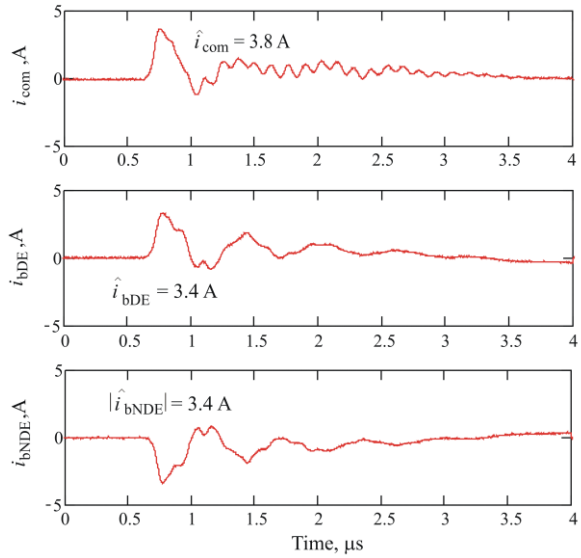

Figure 4. Measured common mode current i_{com} and circulating bearing current at the NDE bearing i_{bNDE} and the DE bearing i_{bDE} for the 110 kW machine M1, fed by a PWM voltage inverter (5 m cable, 560 V DC link voltage, 5 kHz switching frequency), operating at 45 rpm and 60°C bearing temperature.

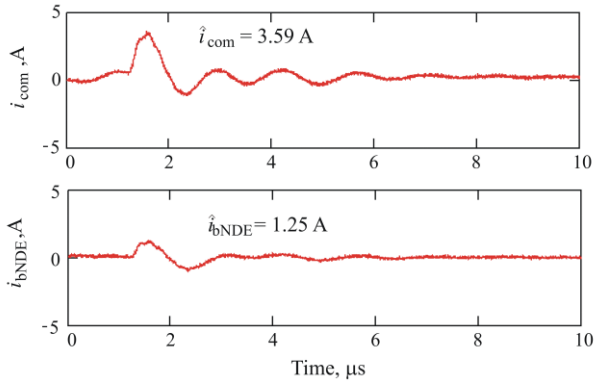

Figure 5. As Fig. 4, but 110 kW machine M2, showing only the common mode current i_{com} and the circulating bearing current i_{bNDE} at the NDE bearing.

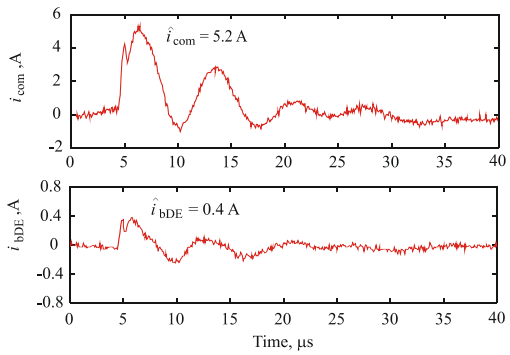

Figure 6. Measured common mode current i_{com} and circulating bearing current i_{bDE} at the DE bearing for the 240 kW machine M3 fed by a PWM voltage inverter (2 m cable, 560 V DC link voltage, 4 kHz switching frequency), operating at 300 rpm and 40°C bearing temperature.

At the same bearing temperature and speed, the tested machines M1 and M2 of Table I of different manufacturers with similar iron core volumes, show similar common mode current amplitudes, but very different bearing current amplitudes. The largest bearing current amplitude was measured for the 110 kW machine M1, which as a difference to the other two tested machines, shows the shorter decay time and the largest oscillation frequency of the common mode current $f_{osc} \cong 1.7$ MHz. The smallest bearing current amplitude was measured for the 240 kW machine, which has the longest decay time and the smallest oscillation frequency of the common mode current $f_{osc} \cong 200$ kHz. The decay time and the oscillation frequency of the common mode current, and of the bearing current as well, depend on the travelling wave effects in the machine winding, thus on the winding configuration. The single layer winding 110 kW machine M1 shows the largest oscillation frequency of the common mode current and therefore the largest induced shaft voltage and the largest bearing current amplitude.

III. Equivalent Circuit Representation

A. Voltage and Current Transformer Models

In order to calculate the circulating bearing current, equivalent eddy-current models, considering the common mode voltage $\underline{U}_{com}$ or the common mode current $\underline{I}_{com}$ as sinusoidal input sources were used in [4] - [6]. At frequencies of 10 kHz … 100 kHz, the impedances of the insulating capacitances between the stator winding and each lamination sheet C_{WS}/N_{lam} are dominating on the common mode current path (Fig. 7). It can be therefore assumed that the common mode current $\underline{I}_{com}$ is distributed linear along the iron core axis and flows in "zigzag" to the ground, through the stator "ground" impedance $\underline{Z}_{Fe,g}$. In [4], [5] the stator ground impedance $\underline{Z}_{Fe,g}$ was considered as half part ($k_d = 0.5$) of the stator laminated core impedance $\underline{Z}_{Fe,b}$:

$$\begin{aligned} \underline{Z}_{Fe,g} &= R_{Fe,g} + j\cdot\omega\cdot L_{Fe,g} = k_d \cdot \underline{Z}_{Fe,b} \\ \underline{Z}_{Fe,b} &= R_{Fe,b} + j\omega\cdot L_{Fe,b} \end{aligned} \quad . \qquad (1)$$

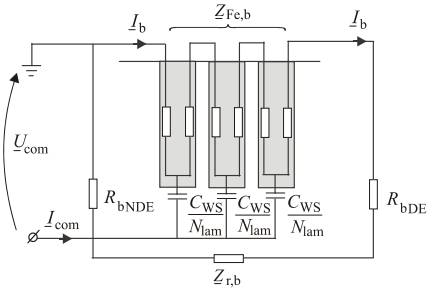

Figure 7. An equivalent transformer model for calculating the circulating bearing current, using the common mode voltage as an input source.

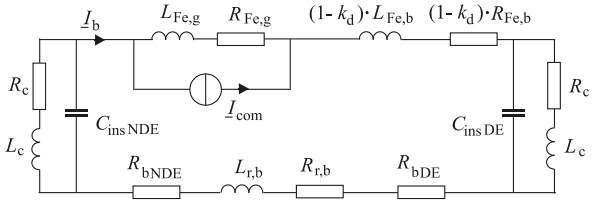

Figure 8. An equivalent transformer model for calculating the circulating bearing current, using the common mode current as an input source. The measurement setup is taken into account by the wire conductor loop resistance and inductance R_c and L_c and the insulating layer capacitances at the DE and NDE bearings $C_{ins\,NDE}$ and $C_{ins\,DE}$.

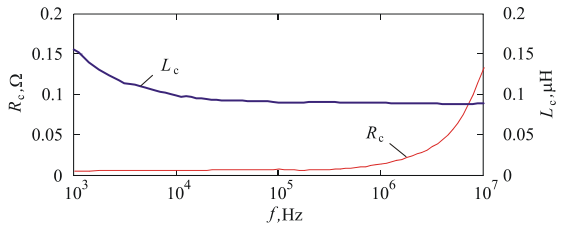

Figure 9. Measured wire conductor loop inductance L_c and resistance R_c.

If the stator resistance $R_{Fe,b}$ and the inductance $L_{Fe,b}$ are rewritten as:

$$\begin{aligned} R_{Fe,b} &= R_{Fe,g} + (1-k_d)\cdot R_{Fe,b} = R_{Fe,g}/k_d \,, \\ L_{Fe,b} &= L_{Fe,g} + (1-k_d)\cdot L_{Fe,b} = L_{Fe,g}/k_d \,, \end{aligned} \qquad (2)$$

the simple current transformer model of Fig. 8 is obtained. Via the inductive coupling, the common mode current $\underline{I}_{com}$ causes the circulating bearing current $\underline{I}_b$ that flows through the stator impedance $\underline{Z}_{Fe,b}$, the rotor impedance

$$\underline{Z}_{r,b} = R_{r,b} + j\omega\cdot L_{r,b} \qquad (3)$$

and the bearing impedances $\underline{Z}_b$. In Fig. 7 and 8, the bearing impedances are represented at the DE and NDE by the resistances R_{bDE} and R_{bNDE}. In [5], the rotor impedance $\underline{Z}_{r,b}$ was considered together with the bearing impedance $\underline{Z}_b \Rightarrow \underline{Z}_{r,b} + \underline{Z}_b$, and in [4] it was considered as a small inductance of the air gap and end-winding cavity $\underline{Z}_{r,b} \approx j\omega\cdot L_{air}$.

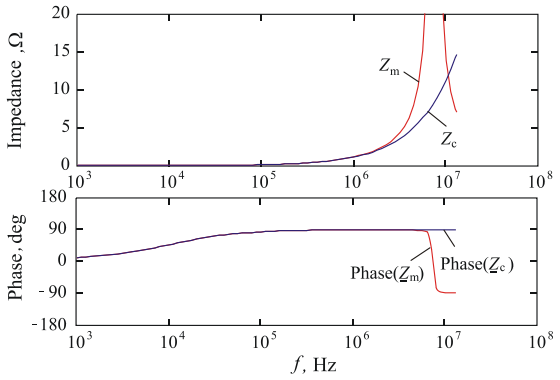

Figure 10. The modulus and the phase of the measurement setup impedance $\underline{Z}_m$ and the copper loop impedance $\underline{Z}_c$.

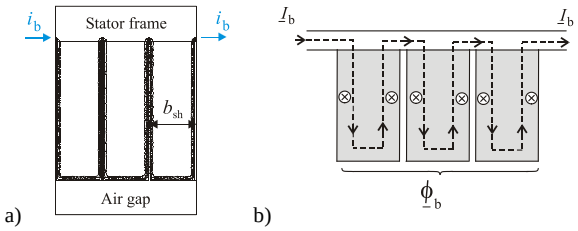

Figure 11. a) - Equipotential magnetic flux lines of the magnetic field at an excitation of 25 kHz, corresponding to an equivalent circulating bearing current distribution, b) – circulating bearing current $\underline{I}_b$ flow and the resulting flux $\underline{\phi}_b$, according to the circulating bearing current theory [4]-[6].

The circulating bearing current is measured via the copper wire conductor loop (Fig. 3). It is represented in Fig. 8 by the resistance R_c and the inductance L_c. Due to the preparing process of the insulating layer, the insulating capacitances at the DE and NDE bearing end-shields may be slightly different. As an example, they are measured for the 110 kW machine M2 of Table I: $C_{insDE} = 5.6$ nF and $C_{insNDE} = 4.8$ nF. The measurement setup impedance of the circulating bearing current path is given as:

$$\underline{Z}_m = \frac{\underline{Z}_c}{1 + j\omega \cdot C_{insDE} \cdot \underline{Z}_c} + \frac{\underline{Z}_c}{1 + j\omega \cdot C_{insNDE} \cdot \underline{Z}_c} \qquad (4)$$

$$\underline{Z}_c = R_c + j\omega \cdot L_c$$

The insulating layer capacitances and the bypass conductor inductances cause a resonance frequency of $f_{res} \cong 7.5$ MHz and cause the increasing impedance $Z_m = |\underline{Z}_m|$ around the resonance frequency (Fig. 10). When the frequency of the circulating bearing current waveform, nearly the same with the frequency of the common mode current waveform f_{osc}, is much smaller than the resonance frequency of the measurement setup, the insulating layer capacitances may be neglected in the equivalent model. Otherwise they affect the measurements, and the insulating layer must be redesigned. Considering the measurement setup impedance $\underline{Z}_m$, the circulating bearing current is calculated from the current transformer model of Fig. 8:

$$\underline{I}_b = \frac{\underline{Z}_{Fe,g} / \underline{Z}_{Fe,b}}{\frac{\underline{Z}_{Fe,b} + \underline{Z}_{r,b}}{\underline{Z}_{Fe,b}} + \frac{R_{bDE} + R_{bNDE}}{\underline{Z}_{Fe,b}} + \frac{\underline{Z}_m}{\underline{Z}_{Fe,b}}} \cdot \underline{I}_{com}. \qquad (5)$$

The internal impedances of the end-shields and of the stator frame are much smaller than the stator core impedance $\underline{Z}_{Fe,b}$, and therefore, they are neglected in (5).

B. Equivalent Circuit Parameters

1) Stator impedance: Due to the skin effect at higher frequencies (> 10 kHz), the circulating bearing current flows in the stator laminated core at the surface of each lamination sheet. The approach is proven here by solving the field problem for three laminations of the 240 kW machine M3, with the thickness of each lamination of $b_{sh} = 0.65$ mm, ideally connected to the frame. At an excitation of 25 kHz, the equipotential flux lines of Fig. 11a are calculated by FEM (finite element methods, FEMM program). They correspond to an equivalent sinusoidal circulating bearing current of 25 kHz, which flows in the stator yoke at the lamination surfaces and prduces a flux $\underline{\phi}_b$ (Fig. 11b), that opposes to the common mode flux. For the field calculation of Fig. 11a, the conductivity of the lamination sheets was taken from the manufacturer data $\sigma_{Fe} = 2.6$ MS/m, and the permeability was chosen $\mu_{Fe} = \mu_r \cdot \mu_0 = 1000\ \mu_0$. The relative permeability $\mu_r = 1000$ is an "incremental" average relative permeability, that validated the circulating bearing current theory [4] - [8]. At frequencies of 10 kHz … 1 MHz, the stator lamination impedance of the circulating bearing current path $\underline{Z}_{Fe,b}$ is calculated analytically for the N_{lam} laminations of the stator yoke [9]:

$$R_{Fe,b} = \frac{P_{tot}}{|I_b|^2} = \frac{N_{lam}}{\pi \cdot \delta_{Fe}} \cdot \frac{1}{\sigma_{Fe}} \cdot \ln\left(\frac{d_{se}}{d_{si} + 2 \cdot h_s}\right), \qquad (6)$$

$$L_{Fe,b} = \frac{R_{Fe,b}}{\omega} = \frac{\mu_{Fe}}{2\pi} \cdot \delta_{Fe} \cdot N_{lam} \cdot \ln\left(\frac{d_{se}}{d_{si} + 2 \cdot h_s}\right), \qquad (7)$$

where the resistance $R_{Fe,b}$ represents the total resistive losses P_{tot}, caused by a sinusoidal circulating bearing current that flows in the stator lamination core, δ_{Fe} is the penetration depth in the iron sheet, σ_{Fe} is the iron conductivity, μ_{Fe} is the iron permeability, h_s is the height of a stator slot, and d_{se} and d_{si} are the stator outer and inner diameters. At frequencies lower than 10 kHz, the inductance $L_{Fe,b}$ has to be calculated using the complex permeability:

$$\underline{\mu}_r = \mu_r \cdot \frac{\tanh\left[(1+j) \cdot b_{sh} / 2\delta_{Fe}\right]}{(1+j) \cdot b_{sh} / 2\delta_{Fe}},$$
$$L_{Fe,b} = \frac{\mu_0}{2\pi} \cdot \mathrm{Re}\left\{\underline{\mu}_r\right\} \cdot l_{Fe} \cdot k_{Fe} \cdot \ln\left(\frac{d_{se}}{d_{si} + 2 \cdot h_s}\right), \qquad (8)$$

where k_{Fe} is the fill factor of the laminated iron core. At frequencies larger than 10 kHz, due to $\mathrm{Re}\{\underline{\mu}_r\} = \mu_r \cdot \delta_{Fe}/b_{sh}$, (7) and (8) give the same results. In order to consider the influence of the axial ventilation ducts, the complex permeability of (8) can be used in the 2D finite element models [10].

The stator inductance $L_{Fe,b}$ and the resistance $R_{Fe,b}$ can be measured with an *RLC*-meter (Fig. 12a). The cable impedance needs to be separately measured and extracted from the total measured impedance of the stator laminated stack and cable. Then, the calculated and measured stator impedances can be compared. For a 1.5 kW 4-pole machine stator core (d_{se} = 147 mm, d_{si} = 90 mm, h_s = 15.2 mm, l_{Fe} = 70 mm and b_{sh} = 0.6 mm), at a conductivity of σ_{Fe} = 3.3 MS/m, taken from the manufacturer data of the lamination sheets, the measured and calculated stator inductances are fitting well for a relative permeability of μ_r = 270 (Fig. 13a, curve 3). The calculated stator resistances $R_{Fe,b} = \omega L_{Fe,b}$ are also fitting well with the measured resistances (Fig. 13b).

2) Rotor impedance: The rotor impedance of the circulating bearing current path appears as a difference of the measured impedances in the conditions of Fig. 12a and Fig. 12b. Fig. 12a allows measurements of the stator impedance, and Fig. 12b allows measurements of the stator and rotor impedance. For the measurements of Fig. 12b, the rotor was introduced inside the stator bore and separated by two small separators at the two stator-ends. Fig. 13a and b (curve 4) show the measured inductances and resistances of the stator and rotor, according to Fig. 12b. They are almost twice larger than the measured stator inductances and resistances of Fig. 12a. In this case, the rotor impedance equals the stator impedance, and we get:

$$\frac{L_{r,b}}{L_{Fe,b}} \cong \frac{R_{r,b}}{R_{Fe,b}} \cong \frac{\underline{Z}_{r,b}}{\underline{Z}_{Fe,b}} \cong 1 \qquad (9)$$

Due to the skin effect in the iron core lamination, the stator inductance and the rotor inductance of the circulating bearing current paths are not mutually coupled, and therefore, they are separately represented in Fig. 8. The manufacturing process of the stator and rotor, the rotor surface tooling to adjust the air gap width, the punching of the lamination sheets with a partial conductive bridging of adjacent iron sheets and the cooling ducts determine a complicated path of the high frequency circulating current and of the high frequency magnetic field in the machine. Thus, the rotor and stator impedances can be only roughly estimated. Furthermore, the shape of the stator slots may have a considerable influence on the rotor impedance. Some improvements in the calculation of the rotor impedance at frequencies larger than 1 MHz are obtained, if the air gap and end-winding cavity inductances are included. The inductance of the air gap and end-winding cavity L_{air} was calculated in [4] from the formula of two series inductances $L_{air,a}$ and $L_{air,b}$ of two coaxial conductors, representing: a) – the air gap zone, framed by the rotor outer diameter d_{re} and the stator inner diameter d_{si}, and b) – the end-winding cavity zone, framed by the rotor inner diameter d_{ri} and the stator outer diameter d_{se} (Fig. 14):

$$L_{air} = L_{air,a} + L_{air,b} = \frac{\mu_0}{2\pi} \cdot \left[l_{Fe} \cdot \ln\left(\frac{d_{si}}{d_{re}}\right) + \left(l_b - l_{Fe}\right) \cdot \ln\left(\frac{d_{se}}{d_{ri}}\right) \right], \qquad (10)$$

where l_{Fe} is the iron core length, and l_b is the distance between the two machine bearings. Since $d_{si} \cong d_{re}$, the inductance of the air gap $L_{air,a}$ is nearly zero and can be neglected, thus $L_{air} \cong L_{air,b}$. The calculated air gap inductance for the 1.5 kW machine is L_{air} = 0.03 µH and for the 240 kW machine M3 is L_{air} = 0.1 µH. The end-shields have only a small influence on the rotor impedance, and therefore they can be also neglected.

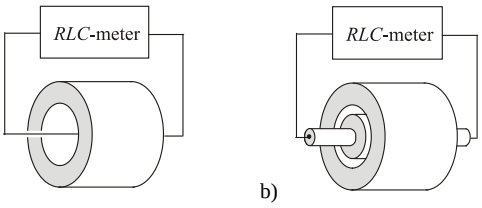

Figure 12. Measurements of a) – stator inductance and b) - stator and rotor inductance.

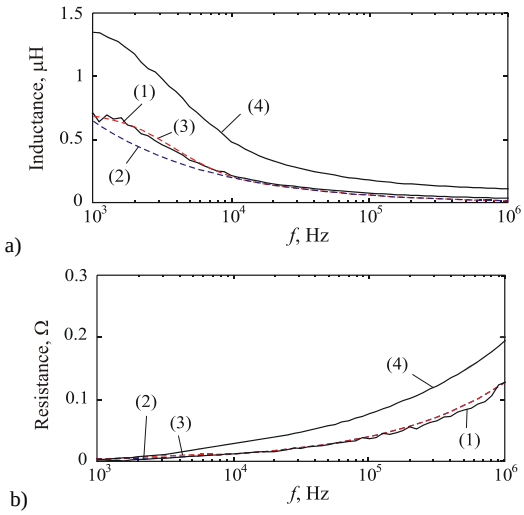

Figure 13. Inductances (a) and resistances (b): 1) – measured according to Fig. 12a, 2) - calculated with eq. (6) and (7), respectively, 3) - calculated with eq. (8), and 4) - measured according to Fig. 12b.

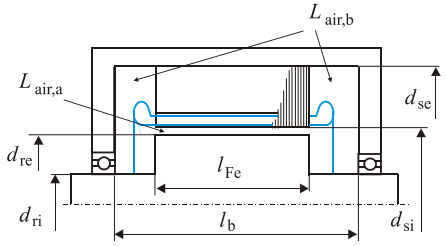

Figure 14. Inductance of the air gap and end-winding cavity.

The rotor and stator inductances increase with an increasing machine size (Fig. 15). In Fig. 15 the measured inductances are given for the 1.5 kW machine of Fig. 13 and for the 240 kW machine M3 of Table III. For each machine, the rotor was separated from the stator by insulated bearings, and the measurements of the rotor and stator impedances were performed by connecting an *RLC*-meter at the two rotor shaft-ends up to a frequency of 50 kHz for the 1.5 kW machine, and a frequency of 100 kHz for the 240 kW machine. Frequencies of 50 kHz and 100 kHz were chosen as maximum limits to avoid the influence of the resonance effects, caused by the insulating layer capacitances.

3) Bearing impedance: At very low speed (< 50 rpm), due to a small thickness of the lubricant film, conductive channels may exist between the bearing lubricated surfaces. The insulating layer of the lubricant film is not complete, and the bearings behave like small resistances in the order of tens of mΩ [1], [4]. With the increasing speed, the lubricant thickness increases and insulates the ball bearings from the bearing raceway. The bearing impedance gets a capacitive behaviour, which reduces the circulating bearing currents. When the transition between the conductive state and the insulating state is done, the EDM (electric discharge machining) currents are likely to occur [1]. However, at speeds around 300 rpm, an intermediate state exists, and circulating bearing currents may pass the machine bearings. Fig. 16 shows the measured average values of 50 peak-to-peak common mode ground currents $i_{\mathrm{com,pp}}$, and the average values of 50 peak-to-peak circulating bearing currents $i_{\mathrm{b,pp}}$ at speeds between 45 rpm and 1500 rpm of the inverter-fed 110 kW machines M1 and M2 of Table I. The common mode current is nearly constant, whereas the circulating bearing current decreases with the increasing speed. For the 110 kW machine M1 (Fig. 16a), the circulating bearing current may reach a peak-to-peak value of 1 A (25% of the common mode current amplitude) even at larger speeds (1500 rpm).

C. Bearing Current Ratio

A bearing current ratio of $BCR = \left|\hat{i}_{\mathrm{b}}/\hat{i}_{\mathrm{com}}\right| \approx \left|i_{\mathrm{b,pp}}/i_{\mathrm{com,pp}}\right| = 0.5..0.9$ was measured at a speed of 45 rpm for the 110 kW machines M1 and M2 (Fig. 16). It shows that the factor $k_{\mathrm{d}} = \underline{Z}_{\mathrm{Fe,g}}/\underline{Z}_{\mathrm{Fe,b}} = 0.5$ cannot be assumed in (5) to predict the circulating bearing current from the common mode current for the 1110 kW machines M1 and M2. The 110 kW machine M1 shows an oscillation frequency of the circulating bearing current of $f_{\mathrm{osc}} = 1.7$ MHz, and the 110 kW machine M2 shows an oscillation frequency of $f_{\mathrm{osc}} = 0.7$ MHz. At these frequencies, the distributed stator winding to stator laminated yoke capacitances $C_{\mathrm{WS}}/N_{\mathrm{lam}}$ are not dominating on the common mode current path, and the common mode current is not distributed linear along the iron core length. At these conditions, a more complicated model is required to calculate the circulating bearing current. However, in the worst case, a rough estimation may assume a bearing current ratio of $BCR \cong 1$, thereby equal amplitudes of the common mode and circulating bearing currents $\hat{i}_{\mathrm{b}} \cong \hat{i}_{\mathrm{com}}$.

IV. Increasing the Rotor Impedance

The standard cage induction machines have low rotor and stator impedances on the circulating bearing current path. At frequencies of 100 kHz … 1 MHz, even the larger machines, as an example the 240 kW machine of Fig. 15, may reach maximum inductances of only 1 µH. Therefore they are exposed to harmful circulating bearing currents. From (5) possibilities for minimizing the circulating bearing currents result directly. If any impedance is added on the rotor shaft, as an example, by mounting a magnetic ring with a high permeability around the shaft (Fig. 17), the circulating bearing current is significantly reduced. Due to $\left|\underline{I}_{\mathrm{b}}/\underline{I}_{\mathrm{com}}\right| \sim \left|\underline{Z}_{\mathrm{Fe,b}}/\left(\underline{Z}_{\mathrm{Fe,b}} + \underline{Z}_{\mathrm{r,b}}\right)\right|$ the method is effective, if the rotor impedance is at least 10 times larger than the stator impedance.

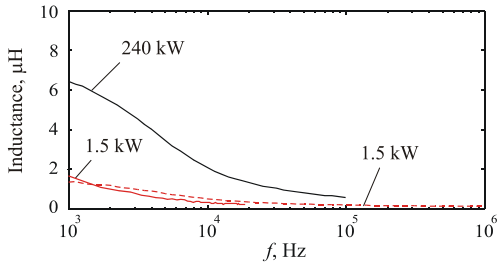

Figure 15. Measured inductances of the 1.5 kW and 240 kW machine. The dashed line is representing the measured inductance of Fig. 13a (4).

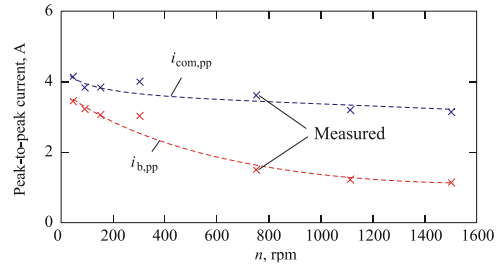

a)

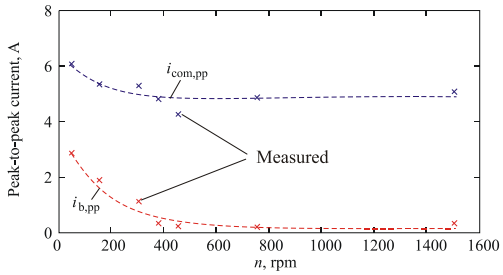

b)

Figure 16. Measured peak-to-peak common mode currents $i_{\mathrm{com,pp}}$ and bearing currents $i_{\mathrm{b,pp}}$ for a) - the 110 kW machine M1 and b) – for the 110 kW machine M2 (Table I), at different speeds and a constant bearing temperature 60°C. The dashed line is the interpolation curve of the measured values.

From the best fitting of the measured stator inductances (Fig. 12a) with the calculated ones by (8), a relative permeability of $\mu_r \approx 300$ was determined for the laminated core of the 1.5 kW induction machine. The measurements of Fig. 15 were done at a very low magnetic field caused by a very low test current of the *RLC*-meter. In the normal operating state, the relative permeability of the laminated core is determined by the amplitude of the fundamental magnetic field, which varies in time and space. An average "incremental" permeability $\mu_r = 1000$ is assumed here to calculate the stator inductances $L_{Fe,b}$. Fig. 18 shows the calculated inductances $L_{Fe,b}$ for the 110 kW machines M1 and M2 and for the 240 kW machine M3 at a relative permeability of $\mu_r = 1000$. The machines have similar iron core volumes and therefore similar stator inductances. At a frequency of $f_{osc} = 1.7$ MHz (circulating bearing current frequency of machine M1), the calculated stator inductance is nearly 0.3 µH. For reducing the circulating bearing currents by up to 10 times, the rotor inductance of the 110 kW machine M1 must be increased up to at least 3 µH, at 1.7 MHz. Here, the 110 kW machine M1 is used as example, because it shows the largest circulating bearing current amplitude from the three tested machines (Fig. 1 ÷ 3).

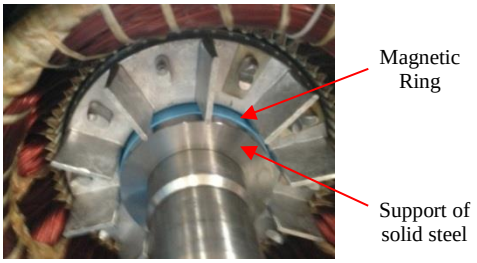

Figure 17. Mounting of the magnetic ring on the 110 kW machine shaft. A support of solid steel is used to fix the magnetic ring on the shaft.

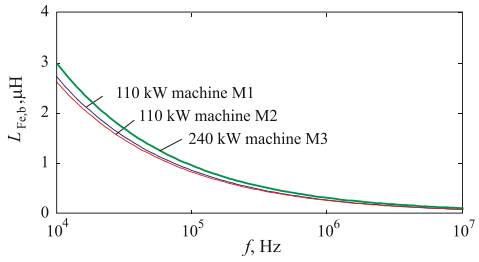

Figure 18. Calculated stator inductances $L_{Fe,b}$ of the machines M1, M2 and M3 of Table I for a relative permeabiltiy of $\mu_r = 1000$.

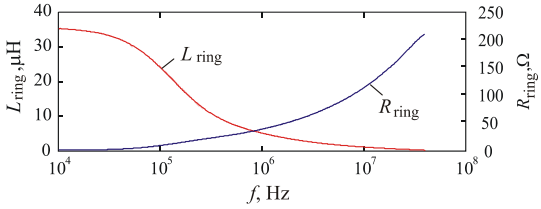

Figure 19. The measured inductance L_{ring} and the resistance R_{ring} of a nanocrystalline magnetic ring type M-190, used for increasing the rotor impedance.

Two identical magnetic nanocrystalline cores, type M-190 (160 mm x 110 mm x 25 mm) with the inductance L_{ring} and the resistance R_{ring} of Fig. 19, which are usually used to reduce the EMI voltage spikes in inverter drive systems [11], [12], are mounted on the machine shaft at the NDE. The rotor inductance is increased up to $L_{r,b} \cong 2 \cdot L_{ring} = 6$ µH, and the machine is operated at 150 rpm. For the standard 110 kW machine M1, the peak-to-peak bearing current of $\hat{i}_b \cong 3.1$ A was measured at 150 rpm (Fig. 16). With the increased rotor impedance, at the NDE bearing the peak-to-peak bearing current is reduced to $\hat{i}_b \cong 0.25$ A (Fig. 20), i.e. with more than 90% of the measured bearing current amplitude of the standard machine. At the non-protected DE bearing, a parasitic bearing current of 0.5 A is still flowing. Since the apparent bearing current density $J_b = \dfrac{\hat{i}_b}{A_{Hz}} = \dfrac{0.5\text{ A}}{10\text{ mm}^2} \cong 0.05\text{ A/mm}^2$ (A_{Hz} denotes the *Hertz*'ian area between the balls and race) is less than the limit for safe operation 0.1 A/mm^2 [3], the machine bearings will not be damaged by the bearing currents. No EDM currents were measured, at any speed, at the NDE bearing where the magnetic ring was mounted. For preventing the occurrence of EDM currents, magnetic shaft rings must be mounted at both the DE side and the NDE side. If a magnetic material is added on the bearing surfaces or/and on the machine end-shield surfaces (near the rotor shaft), not only it reduces the circulating bearing and EDM currents, but it also reduces the rotor-to-ground currents. A future work will present the effectiveness of the nanocrystalline magnetic materials for reducing the EDM and the rotor-to-ground currents.

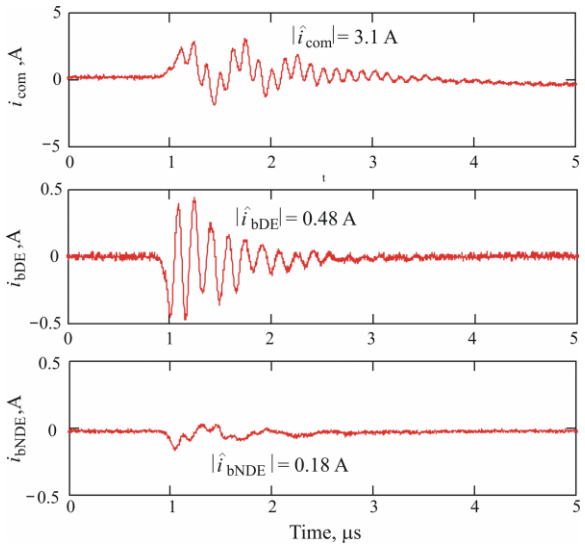

Figure 20. Measured common mode current i_{com} and circulating bearing current at the DE bearing i_{bDE} and the NDE bearings i_{bNDE} for the 110 kW machine M1, operating at 150 rpm, fed by a PWM voltage inverter (5 m cable, 560 V DC link voltage, 5 kHz switching frequency), when a magnetic ring is mounted on the machine shaft at the NDE.

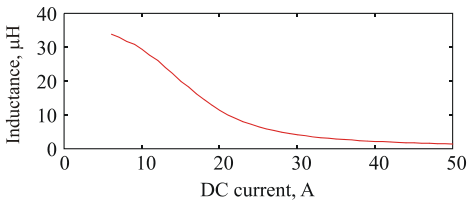

Figure 21. Inductance of nanocrystalline materials with increasing saturation by increased excitation current.

For an effective protection of the machine bearings against the bearing currents, the magnetic shaft ring should operate below the saturation limit, which depends not only on the frequency, but also on the bearing current amplitude. The inductance and resistance characteristics of Fig. 19 are only valid for bearing currents with amplitudes smaller than 10 A. This current limit is given in the material specifications of the core type M-190. At larger currents, the magnetic core saturates, and the impedance of the magnetic ring decreases (Fig. 21). For a proper selection of the magnetic ring, both the amplitude of the circulating bearing current and the stator impedance of the laminated core need to be calculated, estimated or measured. A safe estimation of the circulating bearing current amplitude may assume the worst case of machine operation: $\hat{i}_{\mathrm{b}} \cong \hat{i}_{\mathrm{com}}$. The common mode current amplitude can be measured or calculated beforehand, for example, following the methods of [13] - [18]. An increased temperature of the rotor and of the shaft may change the properties of the magnetic materials. The nanocrystalline materials have operating limits at 180°C … 240°C, which are twice larger than the typical temperatures of the induction cage machine rotor shaft at normal operation.

V. Conclusions

The rotor impedance, due to the circulating bearing current that flows in the stator and rotor laminated cores of the cage induction machines, fed by PWM voltage inverters, is not negligible at high frequency and may be equal to the stator impedance. Generally, the stator and rotor impedances increase with increasing machine size, but even for the larger machines, at frequencies of 100 kHz … 1 MHz, they are in the order of a few ohms only. An increased rotor impedance can mitigate the circulating bearing current, if it is increased by at least ten times the stator impedance. In the case of a 110 kW cage induction machine, a nanocrystalline magnetic material, which was mounted on the machine shaft to increase the rotor impedance, has reduced the amplitude of the circulating bearing current by more than 90% of the measured value of the standard machine.

References

[1] J. Erdman, R. J. Kerkman, D. Schlegel, G. Skibinski, “Effect of PWM Inverters on AC Motor Bearing Currents and Shaft Voltages”, Proc. APEC Conf., vol. 1, pp. 24-33, Dallas, USA, 5-9 March 1995.

[2] D. Dahl, D. Sosnowski, D. Schlegel, R. J. Kerkman, M. Pennings, “Gear Up Your Bearings”, IEEE Ind. Appl. Mag., pp. 45-53, July/August, 2008.

[3] A. Muetze, A. Binder, “Practical Rules for Assessment of Inverter-Induced Bearing Currents in Inverter-Fed AC Motors up to 500 kW”, IEEE Trans. Ind. Elec., vol. 54, no. 3, pp. 1614-1622, January/February 2007.

[4] A. Muetze, A. Binder , “Calculation of Circulating Bearing Currents in Machines of Inverter-Based Drive Systems”, IEEE Trans. on Ind. Electr., vol. 54, no. 2, pp. 932-938, April 2007.

[5] P. Maeki-Ontto, J. Luomi, “Induction motor model for the analysis of capacitive and induced shaft voltages”, Proc. IEMDC Conf., pp. 1653-1660, San Antonio, USA, 11-15 May, 2005.

[6] T. Kovanen, L Soderlund, L. Kettunen, “Mechanism Behind High-Frequency Circulating Bearing Currents in View of Motor Structures”, IET Science, Meas. and Tech., vol. 2, No. 4, pp. 233-243, July 2008.

[7] D. M. Postariu, C. Chillet, J. Roudet, B. Boualem, R. Periot, “Experimental Validation of the Circulating Bearing-Currents Mathematical Theory in the 20 MHz Frequency Range”, Proc. Electromotion – EPE Chapter Joint Symp., 4 pages, CD ROM, July 1-3, Lille, France 2009,

[8] O. Magdun, A. Binder, "An Iron Core Impedance Model for Calculating High Frequency Common Mode Currents and Shaft Voltages in Inverter-Fed AC machines", Proc. SDMEPED Conf., pp. 135-140, June 20-22, Sorrento, Italy, 2012.

[9] P. Maeki-Ontto, J. Luomi, “Common-Mode Flux Calculation of AC Machines”, Proc. ICEM Conf., 6 pages, CD ROM, Bruges, Belgium, 26-28 August, 2002.

[10] A. Muetze, H. De Gersem, T. Weiland, „Influence of Teeth and Cooling Ducts on the High-frequency Common Mode Flux of Inverter-Fed AC Machines“, Proc. IEEE Ind. Appl. Soc. 40th Ann. Meet., 7 pages, CD ROM, Kowloon, Hong Kong, 2-6 October, 2005.

[11] C. R. Sullivan, A. Muetze, “Simulation Model of Common-Mode Chokes for High-Power Applications”, IEEE Trans. Ind. Appl., vol. 46, pp. 884-891, 2010.

[12] M. Ferch, “Softmagnetic Materials in Today's Power Electronic Design”, [online] available on 21.07.2013 at http://www.magnetec.de/en/nanopermr-products.

[13] E. Zhong, T. Lipo, “Improvements in EMC Performance of Inverter-Fed Motor Drives”, IEEE Trans. Ind. Appl., vol. 31, no. 6, pp. 1247-1256, November/December 1995.

[14] B. Mirafzal, G. Skibinski, R. Talam, D. Schlegel, R. Lukaszewski, “Universal Induction Motor Model With Low-to-High Frequency-Response Characteristics”, IEEE Trans. on Ind. Appl., vol. 43, no. 5, pp. 1223-1246, September – October, 2007.

[15] O. Magdun, A. Binder, "The High-Frequency Induction Machine Parameters and their Influence on the CM Stator Ground Current", Proc. ICEM Conf., pp. 503-509, September 2-5, Marseille, France, 2012.

[16] A. Boglietti, E. Carpaneto, “An Accurate Induction Motor High-Frequency Model for Electromagnetic Compatibility Analysis”, Electr. Pow. Comp. and Syst., vol. 29, no. 3, pp. 191-209, March 2001.

[17] R. Cuzner, D. J. Nowak, A. Bendre, G. Oriti, A. L. Julian, "Mitigating Circulating Common-Mode Currents Between Parallel Soft-Switched Drive Systems", IEEE Trans. on Ind. Appl., vol. 43, no. 5, pp. 1284-1294, September/October 2007.

[18] N. Idir, Y. Weens, M. Moreau, and J. J. Franchaud, “High-Frequency Behavior Models of AC Motors”, IEEE Trans. Magn., vol. 45, no. 1, pp. 133-138, January 2009.